Journal of Computational and Applied Mechanics, Vol. 8., No. 2., (2007), pp. 175–191

AN UNSTEADY NUMERICAL SOLUTION OF VISCOUS COMPRESSIBLE FLOWS IN A CHANNEL FOR LOW MACH NUMBERS

Petra Punčochářová*, Karel Kozel**, Jaromír Horáček**,
Jiří Fürst*
*Czech Technical University in Prague
Karlovo náměstí 13, 121 35, Prague 2, Czech Republic
** Institute of Thermomechanics, Czech Academy of Sciences
Dolejškova 5, Prague 8, Czech Republic
puncocha@marian.fsik.cvut.cz

[Received: January 15, 2007]

Abstract. The work deals with the numerical solution of unsteady flow with low Mach numbers in a two-dimensional channel. The flow is described by the unsteady Navier-Stokes equations (laminar) for the compressible fluid. The unsteady flow is caused by a prescribed time periodical motion of a part of the channel wall, which is changing the shape. The numerical solution is realized by the finite volume method and the explicit predictor-corrector MacCormack scheme with Jameson artificial viscosity using a grid of quadrilateral cells. The moved grid of quadrilateral cells is considered in the form of conservation laws using the Arbitrary Lagrangian-Eulerian method. Some numerical results of unsteady flows in a symmetric channel are presented for inlet Mach number $M_\infty = 0.02$, Reynolds number $Re \approx 10^3$ and for frequency of the wall motion 20 Hz. The numerical results were obtained using special software developed by the authors.

Keywords: CFD, FVM, low Mach number, compressible unsteady flow, ALE method, MacCormack numerical scheme

1. Introduction

The work presents a numerical method solving a two-dimensional unsteady compressible viscous flow with low Mach numbers in a symmetric channel. The unsteady flow is caused by a prescribed time periodic motion of a part of the channel wall. The flow in the channel can represent a very simple model of airflow coming from the trachea, through the glottis to the human vocal tract.

In reality, the airflow coming from the human lungs causes the vocal folds' self-oscillations, and the glottis is completely closing in normal phonation regimes generating acoustic pressure fluctuations. In our case, we prescribe a narrow channel harmonic opening and nearly closing the cross-section. The frequency of periodic oscillations of the vocal folds is in most cases higher than 100 Hz. Here, we present

the results with frequency of oscillations 20 Hz. The voice source signal travels from the glottis to the mouth, exciting the acoustic supraglottal spaces and modified by acoustic resonance properties of the vocal tract [1]. Considering the normal speech the airflow velocity in the trachea is approximately in the range $5 - 16$ m/s. Here, we impose a uniform inflow Mach number $M_\infty = 0.02$, i.e., the airflow velocity is 6.68 m/s.

At present, the flow models in the glottis are mostly based on the Bernoulli equation [1] or $1D$ models for the incompressible inviscid fluid [2]. Acoustic wave propagation in the vocal tract is usually modelled separately using the linear acoustic perturbation theory, the wave equation for the potential flow [3]. It is other problematic issue how to model the flow separation point on the moving surface in a small gap. This is usually approximated by some quasi-steady formulas which are deduced from the steady flow solution in divergent channels [4], and the validity of this hypothesis for higher frequencies is questionable. The airflow in the glottis which is described by $2D$ Navier-Stokes equations for the incompressible laminar flow was studied in [5] using the Finite Volume Method (FVM) and in [6] using the Finite Element Method (FEM). Software FIDAP was used in [7] for $3D$ modelling of the flow in glottis by FEM using the Navier-Stokes equations for the incompressible fluid.

When the glottis is closing the airflow velocity becomes much higher in the narrowest part of the airways, where the viscous forces are also important. For the inviscid incompressible flow the maximum flow velocity would tend to infinity just before glottis closure. Therefore for a correct modelling of a real flow in the glottis, the compressible, viscous, unsteady model should be considered. Even if no complete closure of the glottis is modelled, the mathematical model presented for the numerical simulation of the airflow field in the glottis is complex and relatively closer to reality.

The numerical results shown in Section 4 were obtained by the numerical method shown in Section 3 and by the software developed in C/C++, on the basis of the FVM for compressible viscous flow in a narrow channel harmonically opening and nearly closing the cross-section in space and time domains.

2. **Mathematical model**

The $2D$ system of Navier-Stokes equations was used as a mathematical model to describe the unsteady laminar flow of a compressible viscous fluid in a channel. The Navier-Stokes equations are transformed to non-dimensional variables. The transformation of dimensional variables (marked with the accent hat) to the non-dimensional variables is defined as follows:

$$\begin{gathered} \rho \to \hat{\rho}/\hat{\rho}_\infty, \quad (u,v) \to (\hat{u},\hat{v})/\hat{c}_\infty, \quad (x,y) \to (\hat{x},\hat{y})/\hat{L}_s, \quad t \to \hat{t}\cdot\hat{c}_\infty/\hat{L}_s, \\ p \to \hat{p}/(\hat{\rho}_\infty \cdot \hat{c}_\infty^2), \quad e \to \hat{e}/(\hat{\rho}_\infty \cdot \hat{c}_\infty^2), \quad \eta \to \hat{\eta}/\hat{\eta}_\infty, \quad T \to \hat{T}/\hat{T}_\infty, \end{gathered} \tag{2.1}$$

where ρ denotes density, u and v are components of the velocity vector, p denotes static pressure and e is total energy per unit volume. The reference variables in this case are inflow variables (marked with the infinite subscript): speed of sound $\hat{c}_\infty = 334$ m/s, density $\hat{\rho}_\infty = 1.225$ kg/m^3, temperature $\hat{T}_\infty = 293.15$ K, dynamic

viscosity $\hat{\eta}_\infty = 15 \cdot 10^{-6}\ Pa \cdot s$ and a selected length $\hat{L}_s = 0.02\ m$. The system of Navier-Stokes equations is expressed in the non-dimensional conservative form as:

$$\frac{\partial \mathbf{W}}{\partial t} + \frac{\partial \mathbf{F}}{\partial x} + \frac{\partial \mathbf{G}}{\partial y} = \frac{1}{Re}\left(\frac{\partial \mathbf{R}}{\partial x} + \frac{\partial \mathbf{S}}{\partial y}\right), \tag{2.2}$$

where

$$\mathbf{W} = [\rho, \rho u, \rho v, e]^T, \tag{2.3}$$

$$\mathbf{F} = [\rho u, \rho u^2 + p, \rho uv, (e+p)u]^T, \tag{2.4}$$

$$\mathbf{G} = [\rho v, \rho uv, \rho v^2 + p, (e+p)v]^T, \tag{2.5}$$

$$\mathbf{R} = \begin{pmatrix} 0 \\ \frac{2}{3}\eta\left(2\frac{\partial u}{\partial x} - \frac{\partial v}{\partial y}\right) \\ \eta\left(\frac{\partial u}{\partial y} + \frac{\partial v}{\partial x}\right) \\ \frac{2}{3}\eta\left(2\frac{\partial u}{\partial x} - \frac{\partial v}{\partial y}\right)u + \eta\left(\frac{\partial u}{\partial y} + \frac{\partial v}{\partial x}\right)v + k\frac{\partial T}{\partial x} \end{pmatrix}, \tag{2.6}$$

$$\mathbf{S} = \begin{pmatrix} 0 \\ \eta\left(\frac{\partial u}{\partial y} + \frac{\partial v}{\partial x}\right) \\ \frac{2}{3}\eta\left(-\frac{\partial u}{\partial x} + 2\frac{\partial v}{\partial y}\right) \\ \eta\left(\frac{\partial u}{\partial y} + \frac{\partial v}{\partial x}\right)u + \frac{2}{3}\eta\left(-\frac{\partial u}{\partial x} + 2\frac{\partial v}{\partial y}\right)v + k\frac{\partial T}{\partial y} \end{pmatrix}, \tag{2.7}$$

$\mathbf{W}$ is the vector of conservative variables, $\mathbf{F}$ and $\mathbf{G}$ are the vectors of inviscid fluxes, $\mathbf{R}$ and $\mathbf{S}$ are the vectors of viscous fluxes. The static pressure p is expressed by the equation of state:

$$p = (\kappa - 1)\left[e - \frac{1}{2}\rho\left(u^2 + v^2\right)\right]. \tag{2.8}$$

The Reynolds number $Re = \hat{\rho}_\infty \hat{u}_\infty \hat{H}/\hat{\eta}_\infty$ is computed from inflow variables, where $\hat{H} = 2h\hat{L}_s$ is the inflow width of the channel (see Figure 1). The non-dimensional dynamic viscosity found in the dissipative terms of the equations is a function of temperature: $\eta = (T/T_\infty)^{3/4}$. The heat transfer coefficient is expressed as $k = \eta\kappa/[Pr(\kappa - 1)]$, where $Pr = 0.7$ is the Prandtl number and $\kappa = 1.4$ is the Poisson parameter.

2.1. **Mathematical formulation.** For the numerical solution the domain D and the boundary conditions have to be defined.

Figure 1 shows the domain D which represents the symmetric channel. The computational domain is only the lower half of the channel. The upper boundary represents the axis of symmetry. The lower boundary represents the wall and the part of the

channel wall between the points A, B is changing the shape as given function of time and axial coordinate:

$$\begin{aligned} w(x,t) &= \tfrac{1}{2}(a_1+a_t)\cdot\left\{\sin\left[\tfrac{\pi}{C-A}\left(x-\tfrac{A+C}{2}\right)\right]+1\right\}+d, && x\in\langle A,C\rangle,\\ w(x,t) &= \tfrac{1}{2}(a_1+a_t+d)\cdot\left[\cos\left(\pi\tfrac{x-C}{B-C}\right)+1\right], && x\in\langle C,B\rangle,\\ a_t &= a_2\cdot\sin(2\pi f\cdot t), && t\in\langle 0,2\pi\rangle, \end{aligned} \tag{2.9}$$

noindent where $A = [1.75;\ 0.4]$, $B = [2.65;\ 0]$, $C = [2.3;\ w(x = 2.3, t)]$ and the channel geometry has the following non-dimensional parameters: $L = 8$, $h = 0.4$, $d = 0.4$. The frequency of oscillations is computed as $f = 1/(\hat{t}_0 \cdot \frac{\hat{c}_\infty}{\hat{L}_s})$, where $\hat{t}_0 = 0.05\ s$ is the period of oscillations. Then a gap, which is the glottal half-width, can be computed in the following way (see Figure 1): $g(x = 2.3, t) = (d + h) - w(x = 2.3, t)$.

In the work the results for two sizes of the glottal half-widths are presented. The wide glottis has the amplitudes of oscillation (2.9) adjusted to $a_1 = 0.2$, $a_2 = 0.08$ and this case is called the *Wide Gap*. The minimum and maximum of the gap for the *Wide Gap* is: $g_{min} = 0.12$, $g_{max} = 0.28$. In the second case, which is called the *Narrow Gap*, the amplitudes of oscillation are adjusted to $a_1 = 0.3$, $a_2 = 0.08$ and $g_{min} = 0.02$, $g_{max} = 0.18$.

The boundary conditions for the viscous fluid flow have been considered in the following form:

a) Upstream conditions: 3 values of $\mathbf{W}$ are given (ρ, ρu, ρv) and the pressure is extrapolated from the domain to the inlet of the channel, it means $\partial p/\partial \mathbf{n} = 0$ where $\mathbf{n}$ is the outer normal vector to the surface ∂D.
b) Downstream conditions: the pressure p_2 is given and $\partial(\rho,\ \rho u,\ \rho v)/\partial \mathbf{n} = 0$.
c) On the wall the normal derivative of the temperature $\partial T/\partial \mathbf{n} = 0$ and the velocity vector $(u, v)|_{wall} = (0, \bar{v}_{wall})$ are considered. Variable $\bar{v}_{wall}$ is y-velocity component of the lower wall.
d) At the axis of symmetry the condition $(u, v) \cdot \mathbf{n} = 0$ is required.

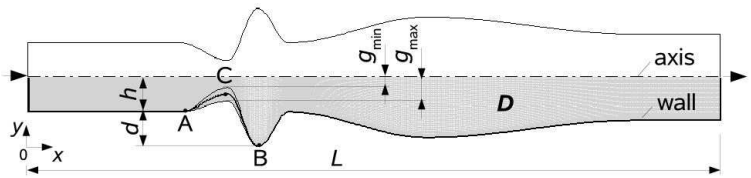

Figure 1. The computational domain D (The symmetric channel)

The shape of this scale model is inspired by the shape of the vocal tract [8]. For the numerical prediction of flow in the vocal tract we used the simplifying assumption that during the normal phonation the vocal fold's oscillations are symmetric [8], hence symmetric geometry is used.

3. **Numerical solution**

3.1. **Algorithm.** The numerical solution of two-dimensional problems uses FVM in cell centred form on a grid of quadrilateral cells.

The bounded domain D is divided into mutually disjoint sub-domains $D_{i,j}$ (e.g. the quadrilateral cells). The equations (2.2) are integrated over the sub-domains $D_{i,j}$ and using the Green formula the following relation is valid:

$$\int_{D_{i,j}} \frac{\partial \mathbf{W}}{\partial t}\, dxdy = -\left[\oint_{\partial D_{i,j}} (\mathbf{F}dy - \mathbf{G}dx) - \oint_{\partial D_{i,j}} (\mathbf{R}dy - \mathbf{S}dx)\right]. \tag{3.1}$$

When the domain is steady, equation (3.1) can be rewritten using the Mean value theorem to the integral form of FVM:

$$\left.\frac{\partial W}{\partial t}\right|_{i,j} = \frac{-1}{\mu_{i,j}}\left[\oint_{\partial D_{i,j}} (\mathbf{F}dy - \mathbf{G}dx) - \oint_{\partial D_{i,j}} (\mathbf{R}dy - \mathbf{S}dx)\right], \tag{3.2}$$

where $\mu_{i,j} = \int\int_{D_{i,j}} dxdy$ is volume of cell $D_{i,j}$. The difference form of FVM is:

$$\frac{\mathbf{W}_{i,j}^{n+1} - \mathbf{W}_{i,j}^{n}}{\Delta t} = \frac{-1}{\mu_{i,j}} \sum_k \left[\left(\tilde{\mathbf{F}}_k - \tilde{\mathbf{R}}_k\right)\Delta y_k - \left(\tilde{\mathbf{G}}_k - \tilde{\mathbf{S}}_k\right)\Delta x_k\right], \tag{3.3}$$

where $\Delta t = t^{n+1} - t^n$ is time step. The physical fluxes $\mathbf{F}, \mathbf{G}, \mathbf{R}, \mathbf{S}$ on an edge k of cell $D_{i,j}$ are replaced by the numerical fluxes (marked with tilde) $\tilde{\mathbf{F}}, \tilde{\mathbf{G}}, \tilde{\mathbf{R}}, \tilde{\mathbf{S}}$ which are approximations of the physical fluxes. The approximations of the numerical fluxes and the time derivative depend on the chosen numerical scheme.

If the domain is unsteady, the integral form of FVM is derived using the Arbitrary Lagrangian-Eulerian (ALE) formulation which defines homeomorphic mapping of the reference domain D_0 at initial time to a domain D_t at time t [9]. Then the equation (3.1) can be written as:

$$\begin{aligned}\int_{D_{i,j|t=0}} \left.\frac{\partial(|J|\mathbf{W})}{\partial t}\right|_{\mathbf{X}_0} d\mathbf{X}_0 = -\Big\{ &\oint_{D_{i,j|t}} (\mathbf{F} - \mathbf{W}\cdot s_1)\, dy - \\ &- (\mathbf{G} - \mathbf{W}\cdot s_2)\, dx] - \oint_{D_{i,j|t}} [\mathbf{R}dy - \mathbf{S}dx]\Big\}.\end{aligned} \tag{3.4}$$

$|J|$ denotes determinant of the Jacobi matrix of the ALE mapping and $\mathbf{X}_0 \in D_0$ is point of reference configuration. In the first integral on the right side fluxes $(-\mathbf{W}\cdot s_i)$ induced by the movement of the boundary of the control volume appear when the ALE method is used. Vector (s_1, s_2) stands for the domain velocity. Hence, the differential form of FVM for unsteady domain is:

$$\begin{aligned}\frac{\mathbf{W}_{i,j}^{n+1}\cdot\mu_{i,j}^{n+1} - \mathbf{W}_{i,j}^{n}\cdot\mu_{i,j}^{n}}{\Delta t} &= -\sum \left[\left(\tilde{\mathbf{F}}_k - s_{1k}\mathbf{W}_k - \tilde{\mathbf{R}}_k\right)\Delta y_k - \right. \\ &- \left.\left(\tilde{\mathbf{G}}_k - s_{2k}\mathbf{W}_k - \tilde{\mathbf{S}}_k\right)\Delta x_k\right].\end{aligned} \tag{3.5}$$

3.2. **Numerical scheme.** For the numerical solution of the system (2.2) the explicit MacCormack (MC) scheme in the predictor-corrector form is used. The scheme is of the 2^{nd} order of accuracy in time and space:

$$\begin{aligned}
\mathbf{W}_{i,j}^{n+1/2} &= \frac{\mu_{i,j}^{n}}{\mu_{i,j}^{n+1}}\mathbf{W}_{i,j}^{n} - \frac{\Delta t}{\mu_{i,j}^{n+1}}\sum_{k=1}^{4}\left[\left(\widetilde{\mathbf{F}}_k^n - s_{1k}\mathbf{W}_k^n - \widetilde{\mathbf{R}}_k^n\right)\Delta y_k - \right.\\
&- \left.\left(\widetilde{\mathbf{G}}_k^n - s_{2k}\mathbf{W}_k^n - \widetilde{\mathbf{S}}_k^n\right)\Delta x_k\right],\\
\overline{\mathbf{W}}_{i,j}^{n+1} &= \frac{\mu_{i,j}^{n}}{\mu_{i,j}^{n+1}}\frac{1}{2}\left(\mathbf{W}_{i,j}^{n} + \mathbf{W}_{i,j}^{n+1/2}\right) - \\
&- \frac{\Delta t}{2\mu_{i,j}^{n+1}}\sum_{k=1}^{4}\left[\left(\widetilde{\mathbf{F}}_k^{n+1/2} - s_{1k}\mathbf{W}_k^{n+1/2} - \widetilde{\mathbf{R}}_k^{n+1/2}\right)\Delta y_k - \right.\\
&- \left.\left(\widetilde{\mathbf{G}}_k^{n+1/2} - s_{2k}\mathbf{W}_k^{n+1/2} - \widetilde{\mathbf{S}}_k^{n+1/2}\right)\Delta x_k\right].
\end{aligned} \tag{3.6}$$

Equation (3.6) represents the MC scheme for the viscous flow in the domain with moving grid of quadrilateral cells. The approximations of the convective terms and the dissipative terms are central and the vector $(s_1, s_2)_k$ represents the speed of edge k (see Fig. 2). The partial derivatives of the velocity and the temperature are approximated using dual volumes V_k' (see [10]) as shown in Figure 2. The partial derivatives of a variable ϕ on the edge k are computed using the following relations:

$$\left.\frac{\partial\phi}{\partial x}\right|_k = \frac{1}{V_k'}\sum_{l=1}^{4}\phi_l\Delta y_l, \quad \left.\frac{\partial\phi}{\partial y}\right|_k = -\frac{1}{V_k'}\sum_{l=1}^{4}\phi_l\Delta x_l. \tag{3.7}$$

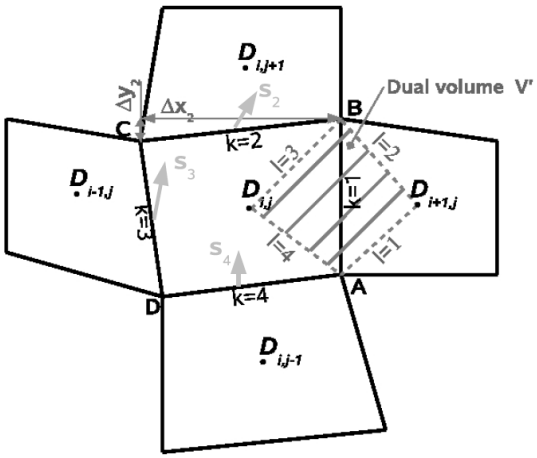

Figure 2. Finite volume $D_{i,j}$, Dual volume $V_k^{'}$

The inviscid numerical fluxes are approximated by the physical inviscid fluxes as follows:

$$\begin{array}{l}
\widetilde{\mathbf{F}}_1^n = \mathbf{F}_{i,j}^n,\ \widetilde{\mathbf{F}}_2^n = \mathbf{F}_{i,j}^n,\ \widetilde{\mathbf{F}}_3^n = \mathbf{F}_{i-1,j}^n,\ \widetilde{\mathbf{F}}_4^n = \mathbf{F}_{i,j-1}^n, \\
\widetilde{\mathbf{G}}_1^n = \mathbf{G}_{i,j}^n,\ \widetilde{\mathbf{G}}_2^n = \mathbf{G}_{i,j}^n,\ \widetilde{\mathbf{G}}_3^n = \mathbf{G}_{i-1,j}^n,\ \widetilde{\mathbf{G}}_4^n = \mathbf{G}_{i,j-1}^n, \\
\text{the corrector step:} \\
\widetilde{\mathbf{F}}_1^{n+1/2} = \mathbf{F}_{i+1,j}^{n+1/2},\ \widetilde{\mathbf{F}}_2^{n+1/2} = \mathbf{F}_{i,j+1}^{n+1/2}, \\
\widetilde{\mathbf{F}}_3^{n+1/2} = \mathbf{F}_{i,j}^{n+1/2},\ \widetilde{\mathbf{F}}_4^{n+1/2} = \mathbf{F}_{i,j}^{n+1/2}, \\
\widetilde{\mathbf{G}}_1^{n+1/2} = \mathbf{G}_{i+1,j}^{n+1/2},\ \widetilde{\mathbf{G}}_2^{n+1/2} = \mathbf{G}_{i,j+1}^{n+1/2}, \\
\widetilde{\mathbf{G}}_3^{n+1/2} = \mathbf{G}_{i,j}^{n+1/2},\ \widetilde{\mathbf{G}}_4^{n+1/2} = \mathbf{G}_{i,j}^{n+1/2}.
\end{array} \tag{3.8}$$

The last term used in MC scheme is the Jameson artificial dissipation $AD(W_{i,j})^n$ [11]:

$$\begin{array}{rcl}
AD(W_{i,j})^n & = & C_1\gamma_1\left(\mathbf{W}_{i+1,j}^n - 2\mathbf{W}_{i,j}^n + \mathbf{W}_{i-1,j}^n\right) + \\
& + & C_2\gamma_2\left(\mathbf{W}_{i,j+1}^n - 2\mathbf{W}_{i,j}^n + \mathbf{W}_{i,j-1}^n\right),
\end{array} \tag{3.9}$$

$C_1, C_2 \in R$ are constants, in our case $C_1 = 1.7,\ C_2 = 1.5$. Normalized pressure gradients $\gamma_1,\ \gamma_2$ have the form:

$$\gamma_1 = \frac{|p_{i+1,j}^n - 2p_{i,j}^n + p_{i-1,j}^n|}{|p_{i+1,j}^n| + 2|p_{i,j}^n| + |p_{i-1,j}^n|}, \quad \gamma_2 = \frac{|p_{i,j+1}^n - 2p_{i,j}^n + p_{i,j-1}^n|}{|p_{i,j+1}^n| + 2|p_{i,j}^n| + |p_{i,j-1}^n|}. \tag{3.10}$$

The use of artificial dissipation is a common way to stabilize the numerical scheme with the higher order of accuracy. The term of artificial dissipation is of the third order of accuracy then the second order of accuracy of the original scheme is valid. Then the vector of conservative variables $\mathbf{W}$ can be computed at a new time level t^{n+1}:

$$\mathbf{W}_{i,j}^{n+1} = \overline{\mathbf{W}}_{i,j}^{n+1} + AD(W_{i,j})^n. \tag{3.11}$$

The stability condition of the scheme (on the regular orthogonal grid) limits the time step:

$$\Delta t \leq CFL\left[\frac{|u_{max}| + c}{\Delta x_{min}} + \frac{|v_{max}| + c}{\Delta y_{min}} + \frac{2}{Re}\left(\frac{1}{\Delta x_{min}^2} + \frac{1}{\Delta y_{min}^2}\right)\right]^{-1}, \tag{3.12}$$

c denotes the local speed of sound, u_{max} and v_{max} are the maximum velocity in the domain, $CFL < 1$ for the non-linear equations. The minimum cell size in y-direction is $\Delta y_{min} \approx 1/\sqrt{Re}$ to resolve capture boundary layer effects (see Fig. 3). The time step in our case mainly depends on $\Delta y_{min} \in (10^{-3}, 2.5 \cdot 10^{-3})$ and the time step during the unsteady problem computation is about $\Delta t \doteq 3 \cdot 10^{-4}$.

4. Numerical results

4.1. **The methods that have been used.** The numerical methods have been suggested and developed at CTU in Prague, Department of Technical Mathematics since 1978. For the Euler and Navier-Stokes equations (compressible and incompressible) methods based on classical schemes as well as modern finite volume schemes (TVD, WENO, AUSM, Residual Distribution Scheme, etc.) have been developed. We tested these methods for laminar and turbulent flows using different types of schemes and grids (structured and unstructured). Also, comparison with experimental results and with other numerical results has been published. The method presented here is also one of the long established and tested methods including the ALE method (see [12]–[19]).

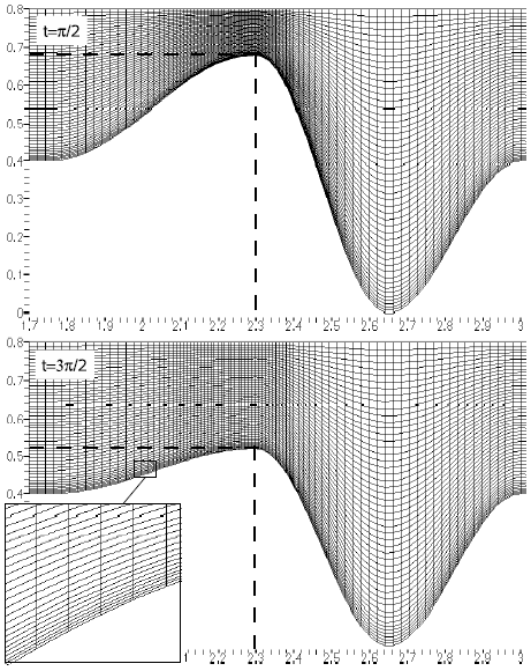

Figure 3. Computational grid in two different time levels (at minimum and maximum of the gap (*Wide Gap*)) and detail of grid refinement near the wall

The method has been tested using a structured grid, refinement of the grid (coarse, fine, very fine) and also very fine grid near walls. The flow has been investigated in three types of channel: in a channel with an upper straight wall and a lower sinus bump time dependent wall using the Euler and Navier-Stokes equations [20], in a divergent axis symmetry channel using the Navier-Stokes equations and in the present type of channel [21], [22].

For the numerical solution, the domain D (see Fig. 1) is covered by a structured grid of quadrilateral cells. Figure 3 shows the grid in part of the channel at two time levels (at minimum and maximum of the gap (*Wide Gap*)). In the detail, the refinement cells near the wall are shown. The computational domain contains 400×50 cells.

The computation of the unsteady solution was carried out in two stages. First, the computation of the steady solution was realized (see Fig. 4(a)). This steady solution was then used as an initial condition for the computation of the unsteady problem, when the unsteady boundary conditions (2.9) are imposed.

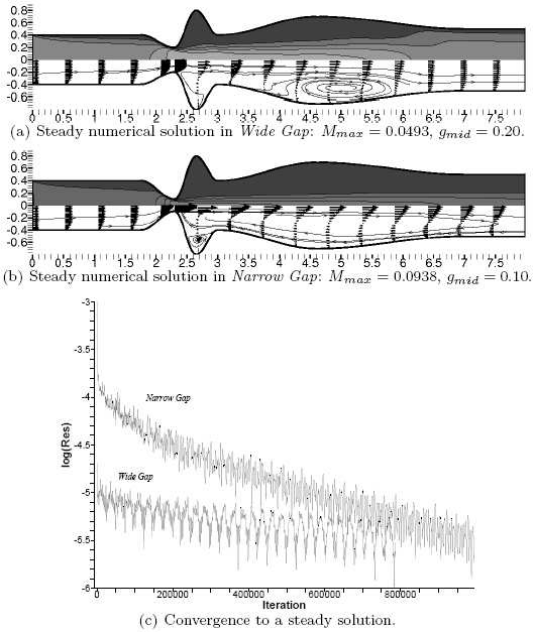

(a) Steady numerical solution in *Wide Gap*: $M_{max} = 0.0493$, $g_{mid} = 0.20$.

(b) Steady numerical solution in *Narrow Gap*: $M_{max} = 0.0938$, $g_{mid} = 0.10$.

(c) Convergence to a steady solution.

Figure 4. Steady numerical solution of viscous compressible (laminar) flow in a symmetric channel. $M_\infty = 0.02$, $p_2 = 1/\kappa$, Re $= 8700$, mesh of 400×50 cells

4.2. **Steady problem.** Figure 4 shows the steady numerical solution for the viscous laminar flow in the domain D (see Fig. 1) with a rigid wall. The gaps are fixed in middle position, for the *Wide Gap* $g_{mid} = 0.20$ and for the *Narrow Gap* $g_{mid} = 0.10$. In both cases the inlet Mach number $M_\infty = 0.02$, the pressure at the outlet $p_2 = 1/\kappa$ and Reynolds number $Re = 8700$. The results are mapped by Mach number iso-lines (upper part of the symmetric channel) and by stream-traces and velocity vectors (lower part of the symmetric channel).

Figure 4(a) shows the steady numerical solution for the *Wide Gap*. The maximum computed value of the Mach number in the domain is $M_{max} = 0.0493$ at point $x =$

2.343 at the channel axis ($y = 0.8$). Figure 4(b) shows the steady numerical solution for the *Narrow Gap*. The maximum Mach number in the domain is $M_{max} = 0.0938$ at the point $x = 2.324$ at the channel axis. Figure 4(c) shows convergence to the steady state solution computed using the L_2 norm of momentum residuals (ρu). The convergence seems to be satisfactory for this very sensitive and complicated cases.

4.3. **Unsteady problem.** Figures 5 and 6 show the unsteady numerical solution of the flow field development of viscous compressible (laminar) flows in a symmetric channel. The results are mapped by Mach number iso-lines (upper part) and by stream-traces and velocity vectors (lower part). In both cases, the inlet Mach number

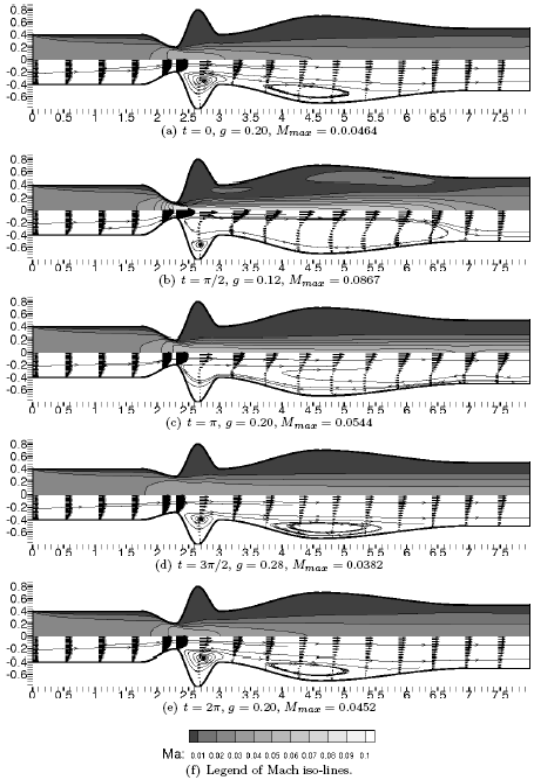

Figure 5. Unsteady numerical solution for the *Wide Gap*. $g_{max} = 0.28$, $g_{min} = 0.12$, $M_\infty = 0.02$, $p_2 = 1/\kappa$, Re $= 8700$, $\hat{f} = 20\ Hz$, mesh of 400×50 cells

$M_\infty = 0.02$, the frequency of oscillations of the wall between the points A, B (see Fig. 1) $\hat{f} = 20\ Hz$, the pressure $p_2 = 1/\kappa$ and $Re = 8700$ are set. The numerical results are shown in the third period of oscillations for the *Wide Gap* and in the second period of oscillations for the *Narrow Gap* at several time layers. Figure 5

shows the numerical solution for the *Wide Gap*. The maximum computed value of the Mach number is $M_{max} = 0.0867$ at the point $x = 2.341$ at the channel axis in time $t = \pi/2$ (see Figs. 5(b) and 9(b)). Figure 6 shows the numerical solution for the *Narrow Gap*. In this case, the highest Mach number was not achieved when the minimum gap was reached as in the previous case, but after the glottal-width began to open. The maximum computed value of the Mach number is $M_{max} = 0.5174$ at the point $x = 2.325$ at the channel axis in time $t = 27/50\ \pi$ (see Fig. 10(b)).

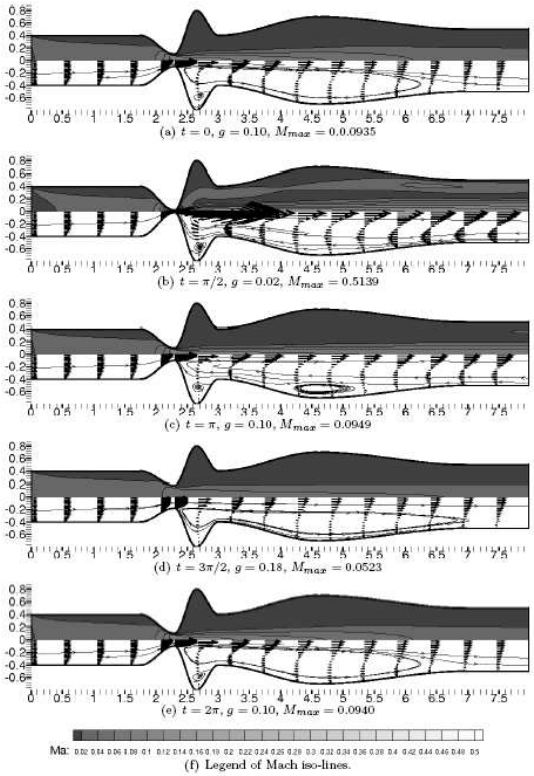

Figure 6. Unsteady numerical solution for the *Narrow Gap*. $g_{max} = 0.18$, $g_{min} = 0.02$, $M_\infty = 0.02$, $p_2 = 1/\kappa$, Re $= 8700$, $\hat{f} = 20\ Hz$, mesh of 400×50 cells

In Figures 7 and 8 the movement of the lower wall $w(x = 2.3, t)$, the pressure and Mach number computed in the narrowest cross-section of the channel at the point $x = 2.3$ at the axis of symmetry in real time domain are shown. Figure 7 shows results of the numerical solution for the *Wide Gap*. It can be seen that after a transition time of about 0.06 s (in the second period of oscillations) the flow becomes almost periodic. Due to a relatively low frequency of oscillations and wide minimal gap, the phase shift between the motion of the wall and the pressure fluctuations is

small. Figure 8 shows results of numerical solution for the *Narrow Gap*. The phase shift between the motion of the wall and the pressure fluctuation is about 0.002 s.

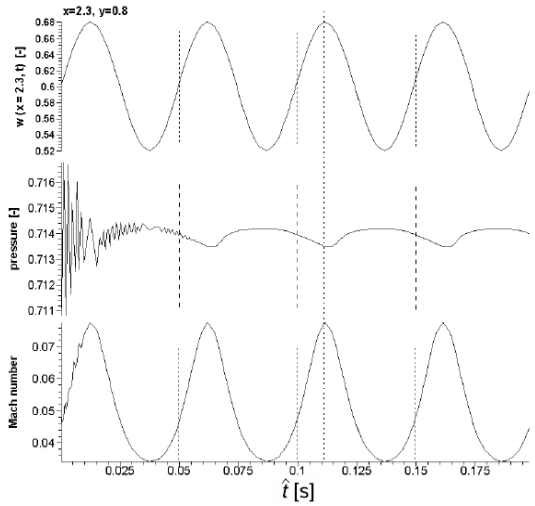

Figure 7. *Wide Gap*. Function of the channel lower wall $w(x = 2.3, t)$, pressure and Mach number computed at the axis of symmetry $(y = 0.8)$, at $x = 2.3$, in real time

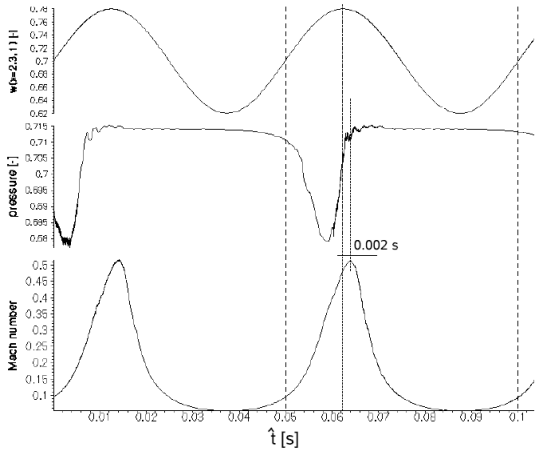

Figure 8. *Narrow Gap*. Function of the channel lower wall $w(x = 2.3, t)$, pressure and Mach number computed at the axis of symmetry $(y = 0.8)$, at $x = 2.3$, in real time

Figures 9 and 10 show the pressure on the wall and the Mach number at the axis of symmetry along the channel at several time levels during one oscillation period. Figure 9 shows the results of the numerical solution for the *Wide Gap*. The minimum of pressure and the maximum of the Mach number are behind the narrowest cross-section of the channel ($x = 2.3$). The highest Mach number appears in time $t = \pi/2$ when the gap is minimal (i.e. $w(x,t)$ is maximal, see the third period in Figure 7). Figure 10 shows the results of the numerical solution for the *Narrow Gap*. In this case the highest Mach number appears after the narrowest cross-section exceeds the minimum of gap (g_{min}), during opening of the glottis, in time $t = 27/50\pi$.

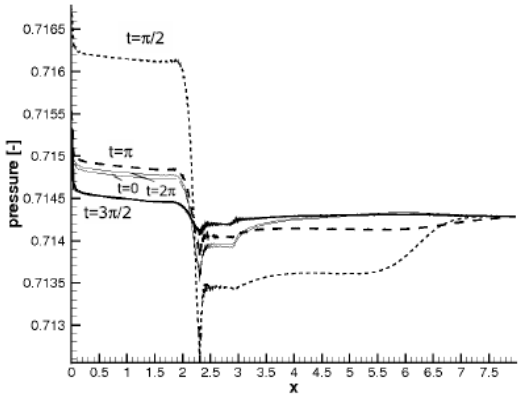

(a) The pressure on the lower wall.

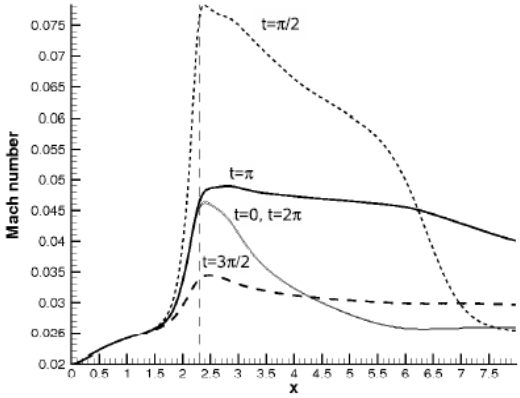

(b) The Mach number at the axis of symmetry.

Figure 9. *Wide Gap*. Pressure on the wall and Mach number at the axis of symmetry along x at several time levels during one oscillation period

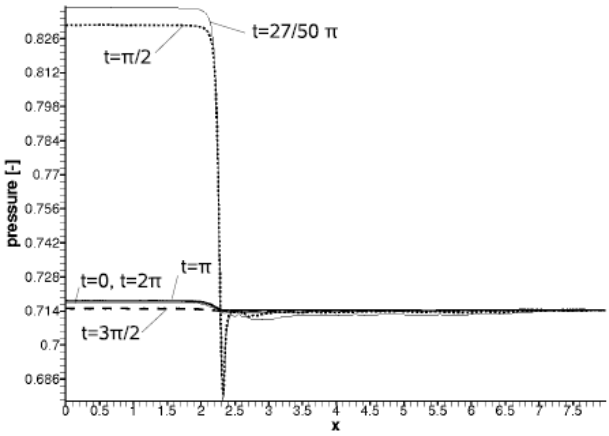

(a) The pressure on the lower wall.

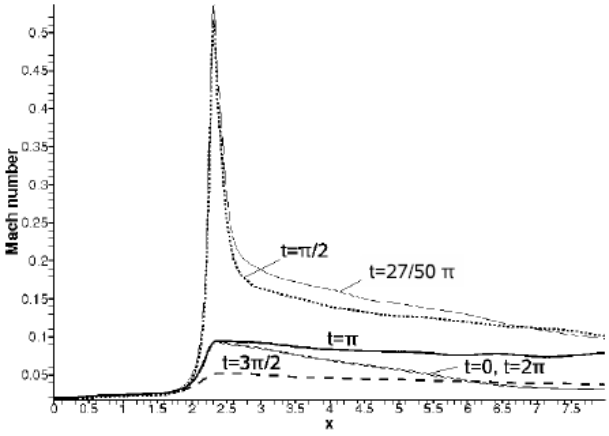

(b) The Mach number at the axis of symmetry.

Figure 10. *Narrow Gap.* Pressure on the wall and Mach number at the axis of symmetry along x at several time levels during one oscillation period

Figure 11 shows the details of the numerical solution for the *Wide Gap* at the point of flow separation in time $t = \pi/2$. The point of flow separation is behind the narrowest cross-section ($x = 2.3$) at about $x_s = 2.33$. The flow separation in a very narrow channel is predicted to occur at the point where the glottal-width ($2g$) exceeds the minimum glottal-width ($2g_{min}$) by $10 - 20$ % [23]. In this case, the distance of the point of separation from the narrowest cross-section is 0.03 and it is 12.5 % of the minimum glottal-width ($2g_{min} = 0.24$). Figure 12 shows the detail of numerical solution for the *Narrow Gap* at the point of flow separation in time $t = \pi/2$. The distance of the point of separation from the narrowest cross-section is 0.016 and it is

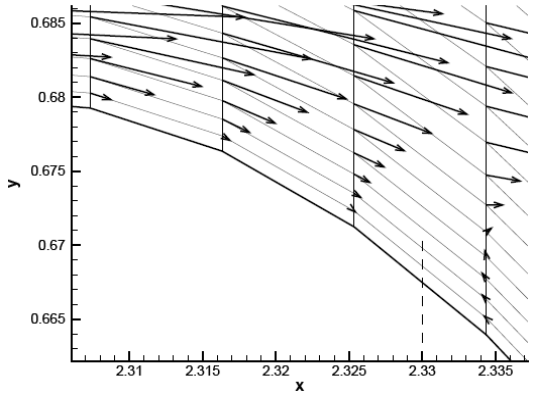

Figure 11. *Wide Gap.* Details of the velocity vectors at the point of flow separation in time $t = \pi/2$ ($g = g_{min} = 0.12$)

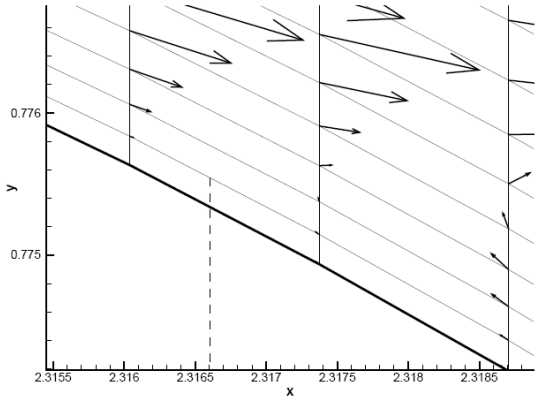

Figure 12. *Narrow Gap.* Details of the velocity vectors at the point of flow separation in time $t = \pi/2$ ($g = g_{min} = 0.02$)

40.0 % of the minimum glottal-width ($2g_{min} = 0.04$) and thus the quasi-steady rule used in [23] is not generally valid. To locate the point of separation in this case, the fine grid around the point of separation is necessary ($\Delta x < 0.001$).

5. **Summary**

A numerical method and a special programme code solving the two-dimensional unsteady Navier-Stokes equations for the viscous compressible fluid has been developed. The method is successfully working for higher Mach numbers (transonic flow) as well as for very low Mach numbers. In the paper this method has been used for the numerical solution of the airflow in a simplified model of the human vocal tract geometry.

The method has been used for two different cases with similar geometry, with the same inlet Mach number M_∞ and frequency of oscillation but with different widths of the narrow part of the channel (*Wide Gap*, *Narrow Gap*). The method can be used successfully in other engineering applications for the steady as well as for the unsteady numerical solution of flows with low Mach numbers, e.g. in studies of other leakage flow-induced vibration problems.

Future tests of the method for applications in modelling of the flow in the human vocal tract will be focused on the higher frequency of oscillation ($\hat{f} \approx 100\ Hz$), the lower inflow Mach number ($M_\infty \leq 0.015$) and on narrower glottal-width ($2g_{min} \leq 0.04$). Also the geometry of the channel will be closer to the real geometry of the glottis and vocal tract.

Acknowledgement. This contribution was partially supported by Research Plan MSM 6840770010 and the projects of GA CR No. 208/08/0012 and GA AS CR No. IAA 200760613.

REFERENCES

1. Titze, I.R.: *Principles of Voice Production*. National Centre for Voice and Speech, Iowa City, 2000, ISBN 0-87414-122-2.
2. Horáček, J., Šidlof, P., and Švec, J.G.: Numerical simulation of self-oscillations of human vocal folds with Hertz model of impact forces. *Journal of Fluid and Structures*, **20**, (2005), 853-869.
3. Titze, I.R.: *The Myoelastic Aerodynamic Theory of Phonation*. National Centre for Voice and Speech, Iowa City, 2006, ISBN 0-87414-122-2.
4. Pelorson, X., Hirschberg, A., van Hassel, R.R., Wijands, A.P.J. and Auregan, Y.: Theoretical and experimental study of quasisteady-flow separation within the glottis during phonation. *Journal of the Acoustical Society of America*, **96**, (1994), 3416-3431.
5. Alipour, F. and Titze, I.R.: *Combined simulation of two-dimensional airflow and vocal fold vibration*. P.J. Davis, N.H. Fletcher (Eds.), Vocal Fold Physiology, Controlling Complexity and Chaos. Singular, San Diego, 1996.
6. De Vries, M.P., Schutte, H.K., Veldman, A.E.P. and Verkerke, G.J.: Glottal flow through a two-mass model: Comparison of Navier-Stokes solutions with simplified models. *Journal of the Acoustical Society of America*, **111**(4), (2002), 1847-1853.
7. Rosa, M.O. and Pereira, J.C.: A contribution to simulating a three-dimensional larynx model using the finite element method. *Journal of the Acoustical Society of America*, **114**(5), (2003), 2893-2905.
8. Dedouch, K., Horáček, P. and Švec, J.G.: *Frequency modal analysis of supraglottal vocal tract*. N. S. Ferguson, H. F. Wolfe, M. A. Ferman, S. A. Rizzi (Eds.), Structural Dynamics: Recent Advances. University of Southampton, England, 2000, pp. 863-874, ISBN 0854327215.
9. Honzátko, R., Kozel, K., and Horáček, J.: Flow over a profile in a channel with dynamic effects. *Proceedings in Applied Mathematics*, **4**(1), (2004), 322-323. ISSN 1617-7061.

10. Fürst, J., Janda, M. and Kozel, K.: Finite volume solution of 2D and 3D Euler and Navier-Stokes equations. J. Neustupa, P. Penel (Eds.), Mathematical Fluid Mechanics. Berlin, (2001). ISBN 3-7643-6593-5.

11. Jameson, A., Schmidt, W., and Turkel, E.: Numerical Solution of the Euler Equations by Finite Volume Methods Using Runge-Kutta Time-Stepping Schemes, AIAA, Paper 81-1250, (1981).

12. Fořt, J. and Kozel, K.: Numerical solution of several models of internal transonic flow. *Applications of Mathematics*, 8(6), (2003), 515-524. ISSN 0862-7490.

13. Kozel, K., Louda, P. and Sváček, P.: Numerical Solution of Flow in Backward Facing Step, Numerical Mathematics and Advanced Applications, ENUMATH 2003, (2004), Berlin, pp. 596-604.

14. Dobeš, J., Fořt, J., Fürst, J., Halama, J. and Kozel, K.: Numerical Solution of Transonic Flows in Turbine Cascades, 1st International Conference FSCCE. Athens, 2004.

15. Prokop, V. and Kozel, K.: Numerical Modelling of Bypass Flow. Numerical Mathematics and Advanced Application. Berlin, (2004), pp. 708-715. ISBN 3-540-21460-7.

16. Kozel, K., Louda, P. and Příhoda, J.: Numerical Modelling of Complex Turbulent Flows, Proceedings of "16th International Symposium on Transport Phenomena", CD-ROM, CTU in Prague, (2005).

17. Kozel, K., Honzátko, R. and Horáček, J.: Numerical Solution of 2D Incompressible Flow over a Vibrating Airfoil, Proceedings of Conf. On Modelling Fluid Flow, Budapest, (2006), pp. 233-240, ed. T. Lajos, J. Vad. ISBN 963 06 0361 6.

18. Šimonek, J., Kozel, K. and Trefilík, J.: Numerical Solution of Inviscid and Viscous Flows with Application, Topical Problem of Fluid Mechanics (2007). Prague, IT CAS CZ, 2007, pp. 169-172. ISBN 978-80-87012-04-8.

19. Punčochářová, P., Kozel, K. and Fürst, J.: An unsteady numerical solution of viscous compressible flows in a channel, Programs and Algorithms of Numerical Mathematics 13. Prague, Math. Institute ASCR, (2006), pp. 220-228. ISBN 80-85823-54-3.

20. Punčochářová, P., Kozel, K. and Fürst, J.: Unsteady, Subsonic Inviscid and Viscous Flows in a Channel, Fluid Dynamics 2005. Prague, IT CAS CZ, (2005), pp. 125-128. ISBN 80-85918-94-3.

21. Punčochářová, P., Kozel, K., and Fürst, J.: Numerical Solution Viscous Flows in a 2D Channel with Unsteady Wall Boundary, Application of Experimental and Numerical Methods in Fluid Mechanics. University of Žilina, Mechanical Engineering Faculty, 2006, 177-182. ISBN 80-8070-533-X.

22. Punčochářová, P., Kozel, K., Fürst, J., and Horáček, J.: Numerical Solution of Unsteady Viscous Compressible Flows in a Channel, Topical Problem of Fluid Mechanics 2006. Prague, IT CAS CZ, 2006, pp. 133-136. ISBN 80-85918-98-6.

23. Lous, N.J.C., Hofmans, G.C.J., Veldhuis, N.J. and Hirschberg, A.: A symmetrical two-mass model vocal-fold model coupled to vocal tract and trachea, with application to prosthesis design. *Acta Acoustica*, **84**, (1998), 1135-1150.